Palladium Supported on 3D Graphene as an Active Catalyst for Alcohols Electrooxidation

Alexey Serov,[a,*] Nalin I. Andersen,[a] Sadia A. Kabir,[a,] Aaron Roy,[a] Tristan Asset,[b,c] Marian Chatenet,[b,c,*] Frederic Maillard,[b,c,*] and Plamen Atanassov[a,*,z]**

[a]*Department of Chemical & Biological Engineering and Center for Micro-Engineered Materials (CMEM), The University of New Mexico, Advanced Materials Laboratory, Albuquerque, New Mexico 87131, USA*
[b]*University of Grenoble Alpes, LEPMI, F-38000 Grenoble, France*
[c]*CNRS, LEPMI, F-38000 Grenoble, France*

In the present study, highly porous 3D-Graphene nanosheets (3D-GNS) were synthesized using the Sacrificial Support Method (SSM) and utilized as a support for palladium (Pd) nanoparticles. The Pd nanoparticles were deposited using the original Pd-precursor based Soft Alcohol Reduction Method (SARM) with different alcohols. The obtained materials were comprehensively characterized by X-ray diffraction (XRD), transmission electron microscopy (TEM), and scanning transmission electron microscopy (SEM). Chemically reduced Pd/3D-GNS catalysts were then studied for the electrochemical oxidation of ethanol and methanol in alkaline media. Our study shows that combination of SSM and SARM-EtOH fabrication process allowed obtaining materials with a smaller particle size distribution and a higher surface area (yielding better utilization of Pd), as well as the highest electrochemical activity and durability, with a peak current density of over 1100 A/g_{Pd} for ethanol electrooxidation.
 [DOI: 10.1149/2.0301512jes] All rights reserved.

Manuscript submitted July 6, 2015; revised manuscript received August 20, 2015. Published August 28, 2015.

The development of high-performance anion-exchange ionomers and membranes by the Tokuyama Corp. and FuMa-Tech GmbH. resulted in an increased interest toward Direct Liquid Fed Fuel Cells (DLFFC). Examples of DLFFCs are Direct Methanol Fuel Cells (DMFC),[1] Direct Ethanol Fuel Cells (DEFC),[2] Direct Ethylene Glycol Fuel Cells (DEGFC),[3] Direct Formic Acid Fuel Cells (DFAFC),[4] Direct Hydrazine Fuel Cells (DHFC),[5] Direct Dimethyl Ether Fuel Cells (DDEFC)[6] and Direct Sodium Borohydride Fuel Cells (DSBFC).[7]

The usage of liquid fuels and anion-exchange membranes (AEM) has substantial advantages in comparison to the hydrogen-fed proton-exchange membrane technology. For example, liquid fuels have higher gravimetric and volumetric energy densities where the logistics of fuel delivery are much simpler in comparison to compressed hydrogen. Moreover, the electro-oxidation kinetics for many liquid fuels is enhanced in alkaline environment. Note also that the oxygen reduction reaction (ORR) kinetics is faster in alkaline media than in acidic ones, and that the migration of OH^- anions from the anode to the cathode compartment of the fuel cell results in a reduced crossover of liquid fuels. These advantages enable to use relatively cheaper non-precious materials for both anodes and cathodes[9] have been reviewed by Antolini et al.[8]

The higher activity of Pd and Pd-based catalysts in alkaline media for alcohols electrooxidation reaction in comparison to platinum (Pt) is well-established and reviewed by several research groups.[10–23] In order to better utilize the Pd nanoparticles, supported and nanostructured catalysts should be used. The support should meet certain requirements such as a high surface area, excellent electrical conductivity, and provide good contact to the metal nanoparticles. Presently, carbonaceous materials such as carbon blacks, nanotubes, nanofibers, etc. are of the most extensively used materials for catalytic support; however, the majority of these carbon supports have a substantial amorphous component, which is less conductive than graphite and presents durability issues.[24] On the other hand, highly graphitic materials usually have a low surface area. The common problem for both amorphous and graphitic materials is the weak interaction of noble metal nanoparticles with the surface, which eventually leads to particle detachment and a decrease in the catalyst durability (see e.g.[24–28])

In order to overcome these limitations, we report the synthesis of highly defective 3D graphene nano-sheets (3D-GNS) with high surface area, which was implemented as a support for Pd nanoparticles. The deposition of Pd was achieved by the original Soft Alcohol Reduction Method (SARM), which does not use any reducing agents, except for the solvent itself. Three different novel catalysts were synthesized using ethanol (EtOH), methanol (MeOH) and isopropyl alcohol (IPA), and comprehensively characterized using different surface-analysis techniques and cyclic voltammetry.

Experimental

Preparation of 3D-GNS by the sacrificial support method (SSM).— Preparation of 3D-GNS began with the synthesis of graphene oxide (GO) by the modified Hummers method.[29] As-prepared graphene oxide was stored in its wet form and used for further synthesis. The synthesized GO was fully exfoliated in a water solution using a high power ultrasonic probe (600 kJ were delivered to 10 g of GO in 1 L of de-ionized (DI) water for 2 h) followed by the addition of 20 g of EH-5 fumed silica (Cab-O-Sil, surface area $\approx 400\ m^2\ g^{-1}$). The mixture of GO-SiO_2 was ultrasonicated with the probe for 1 more hour and dried overnight at $T = 85°C$. Dry powder was ball-milled at 400 RPM for 15 min and subjected to reduction in 7% H_2 (flow rate = 100 ccm) at $T = 800°C$ for 1 h. After reduction, this hybrid of GNS-SiO_2 was ball-milled at 400 RPM for 15 min. The silica support was leached by means of 25 wt% HF for 24 h, followed by continuous filtration until a neutral pH was achieved. The resulting 3D-GNS was dried overnight at $T = 85°C$ and its powdered form was doped with nitrogen in 10% NH_3 (flow rate = 100 ccm) at $T = 850°C$ for a duration of 2 h. The subsequent 3D-GNS was used as a support material for Pd deposition.

Pd deposition on 3D-GNS by soft alcohol reduction method (SARM).— 1 g of 3D-GNS was dispersed in the alcohol of choice (MeOH, EtOH or IPA) using a high-energy ultrasonic probe. A calculated amount of $Pd(NO_3)_3{}^*2H_2O$ (in order to get 30 wt% on 3D-GNS) was dissolved in water (in order to get a 50:50 final mixture, by volume with the alcohol of choice) and added to the 3D-GNS while sonicating for 15 min and centrifuged. The black precipitate was washed twice with DI water followed by a washing with the alcohol of choice twice. The mixture was dried to a powder at $T = 85°C$ overnight. In order to compare the activity of Pd on 3D-GNS with 2D-Graphene (2D-GNS), dried GO was thermally reduced in 7% H_2 followed by 10% NH_3 without using silica as a template. In addition, 30 wt% Pd was deposited on a conventional carbon black support, i.e. XC72R (Cabot, Vulcan XC72R) for reference. General synthesis approach is depicted in Figure 1.

*Electrochemical Society Active Member.
**Electrochemical Society Student Member.
[z]E-mail: plamen@unm.edu

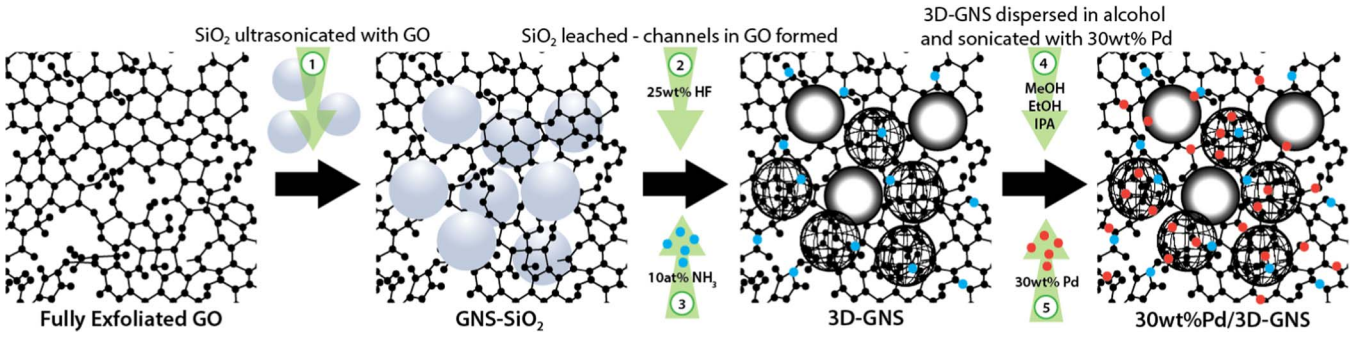

Figure 1. The schematic representation of the synthesis route for Pd/3D-GNS.

Physical characterizations.— The morphologies of the synthesized materials were determined by scanning electron microscopy (SEM, Hitachi S-5200 Nano SEM with an accelerating voltage of 10 keV) and transmission electron microscopy (TEM, JEOL 2010 instrument with an accelerating voltage of 200 keV). Powder X-ray diffraction (XRD) analysis was performed using a Rigaku Smartlab diffractometer with Bragg-Brentano focusing geometry. The X-ray source used was a Cu anode operating at 40 kV and 40 mA. The detector used was the Rigaku D/teX Ultra 250 1D silicon strip detector with a K-β incident beam monochromator. Surface areas were measured by N_2-sorption (Brunauer–Emmett–Teller method, BET), using a Micrometrics 2360 Gemini Analyzer.

Electrochemical characterization.— The electrochemical analyses of the synthesized materials were performed using the Pine Instrument Company electrochemical analysis system. The rotational speed was $\omega = 600$ RPM, and the potential scan rate $\nu = 20$ mV sec^{-1}. The electrolyte was 1 M KOH saturated in N_2 at room temperature. A Pt wire counter-electrode and a Hg/HgO reference electrode were used. The working electrodes were prepared by mixing 5 mg of the 30 wt% Pd/3D-GNS (or 2D-Graphene and Vulcan for comparison) electrocatalyst with 925 μL of a water and isopropyl alcohol (4:1) mixture, and 75 μL of Nafion (0.5 wt% solution, DuPont). The mixture was sonicated before 10 μL was applied onto a glassy carbon disk with a sectional area of 0.2472 cm^2. The catalyst loading on the electrode was 0.2 mg cm^{-2}. Electrooxidation of 1 M MeOH and 1 M EtOH was studied on the synthesized Pd/3D-GNS and Pd/2D-GNS catalysts and their durability compared by chronoamperometry method.

Results and Discussion

Effect of the sacrificial template on surface morphology.— Morphological analysis of the 3D-GNS was performed by SEM (Figure 2). It can clearly be seen that the synthesized 3D graphene material has numerous defects and large pores (Figure 2Ai). The latter were formed after removal of the silica support. It should be mentioned that the number of pores can be controlled by the ratio between the graphene oxide and the silica, while the pore diameter can be varied by changing the silica type. The surface area of the 3D-GNS was found to be around 450 m^2 g^{-1}, which is substantially higher than graphite material (around 1–5 m^2 g^{-1}). In contrast, the 2D-Graphene (2D-GNS) had a significantly lower surface area of 100 m^2 g^{-1}. The difference in surface areas between the two graphene supports could be due to the lack of a mesoporous morphology in 2D-GNS as shown in Figure 2Aii. In 3D-GNS, pores were formed when SSM sacrificial template (SiO_2) was leached out using HF. This porous nature of 3D-GNS can enhance mass diffusion and transport through pores and improve catalytic activity. However, 2D-GNS supports were synthesizing without utilizing a sacrificial support. The morphology of its basal planes are therefore non-porous, reducing its overall surface area.

Effect of solvent on particle size and distribution.— In the Soft Alcohol Reduction Method, the reduction of Pd precursors is performed by the solvent. In the present work, we investigated the influences of the morphology and electrocatalytic activity of Pd nanoparticles with the following alcohols: methanol, ethanol, and iso-propyl alcohol. A volumetric ratio of 1:1 between alcohol and water was selected. Prior to the deposition of Pd on 3D-GNS, model experiments were performed without the addition of any substrates into the Pd precursor solution. The fastest reduction of Pd nitrate was in the case of EtOH addition, wherein the solution turned black within 5 seconds. The second fastest alcohol for Pd nitrate reduction was for IPA where the solution was still brown after 5 minutes (see Figure 3). The slowest

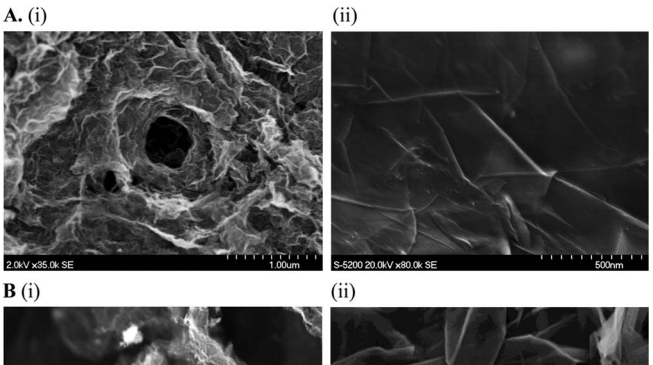

Figure 2. SEM Images of thermally reduced A) (i) 3D-GNS prepared by Sacrificial Support Method and (ii) 2D-GNS prepared without a sacrificial support; B) (i) Pd/3D-GNS and (ii) 2D-GNS prepared by SARM-EtOH.

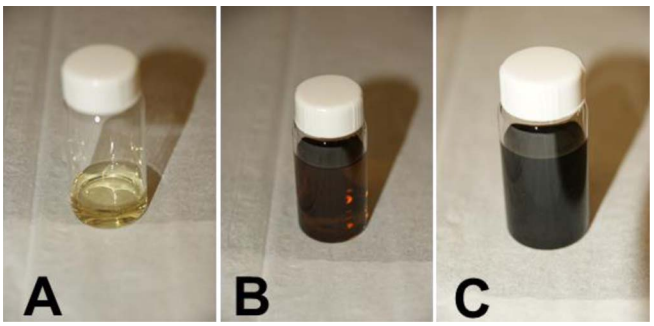

Figure 3. $Pd(NO_3)_2{}^*2H_2O$ reduced by IPA using the Soft Alcohol Reduction Method: (A) Pd nitrate solution in water, (B) 5 minutes after addition of IPA and (C) 1 hour after addition of IPA.

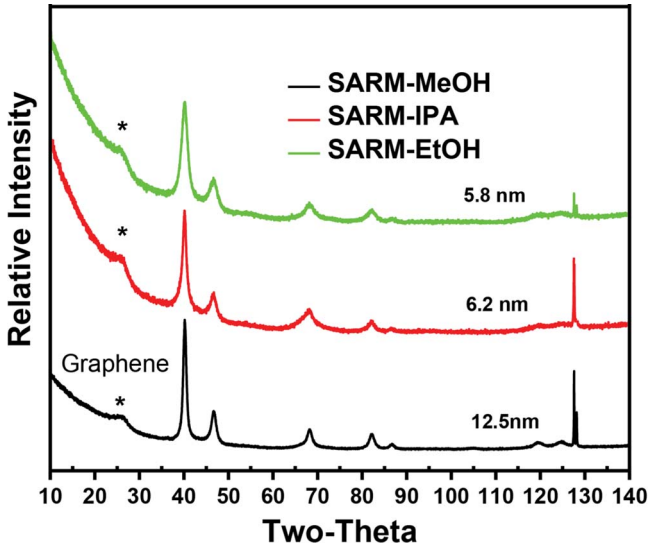

Figure 4. X-ray diffractograms of different 30 wt% Pd/3D-GNS materials.

reduction was found in the case of MeOH, where the solution remained in a state of a semi-transparent pale-brown beyond 15 minutes.

After washing and drying, the synthesized Pd/3D-GNS samples were characterized by XRD and TEM. Analysis of XRD patterns revealed the complete reduction of Pd nitrate into Pd^0 (Figure 4). We did not observe any other materials in the samples aside from graphene and metallic Pd. The dispersed state of the Pd/3D-GNS particles synthesized using EtOH, IPA and MeOH and corresponding histogram of their particle size distribution obtained from TEM is displayed in Figures 5a and 5b. Pd/3D-GNS-EtOH and Pd/3D-GNS-IPA had an average particle diameter of 4.3 ± 1.2 nm and 5.1 ± 1.4 nm respectively, whereas Pd/3D-GNS-MeOH particles were ~6 times bigger, with an average particle diameter of 31.2 ± 3.0 nm. This can be explained by the relative reduction power of the alcohols in the order of EtOH > IPA > MeOH. Indeed, due to its high reduction power, the use of EtOH resulted in larger amounts of nuclei, and due to the fact that the concentration of precursors is finite and large (high degree of supersaturation), the growth of those initial nuclei remained limited (in other words, more numerous and smaller nanoparticles of ~4nm are formed for EtOH). In the case of MeOH, fewer nuclei were formed, which continued to grow up to an average of 30nm with time. Analysis of TEM images (Figure 5) confirmed this scenario at the support scale: the materials derived from SARM-EtOH and SARM-IPA consisted of 3D-GNS evenly populated by non-agglomerated Pd nanoparticles, whereas the material obtained from SARM-MeOH consisted of large Pd nanoparticles agglomerated from smaller ones, which could explain the difference between TEM observation (Fig. 5aiii) and XRD analysis (Fig. 4).

Effect of carbon support on catalytic activity.— It is well known that the synthesis of graphene oxide is quite complicated due to the fact that the material should be washed from manganese salts. That procedure is time consuming, not scalable, and requires special vacuum set-ups or osmotic systems; these factors lead to small batches and high prices for the final product. In the methods presented here, the number of washing step can be kept as low as one or two, because all organic material will evaporate during the reduction step and all unreacted manganese will dissolve in HF during the silica leaching step. This simplification results in increasing the batch size for lab-scale up to 20 g, at a reasonable process cost.

Electrochemical performance of Pd/3D-GNS materials in comparison with Pd/2D-GNS and Pd/XC72R in the electrooxidation of methanol or ethanol is displayed in Figures 6 and 7. In both of the ethanol and methanol electrooxidation experiments, the most active material was derived from SARM-EtOH. This can be explained by the small size and the even dispersion of the Pd particles on the surface of the 3D-GNS. The SARM-MeOH sample was the less efficient (it was even less active than the reference Pd/XC72R for ethanol oxidation, Figure 6B).

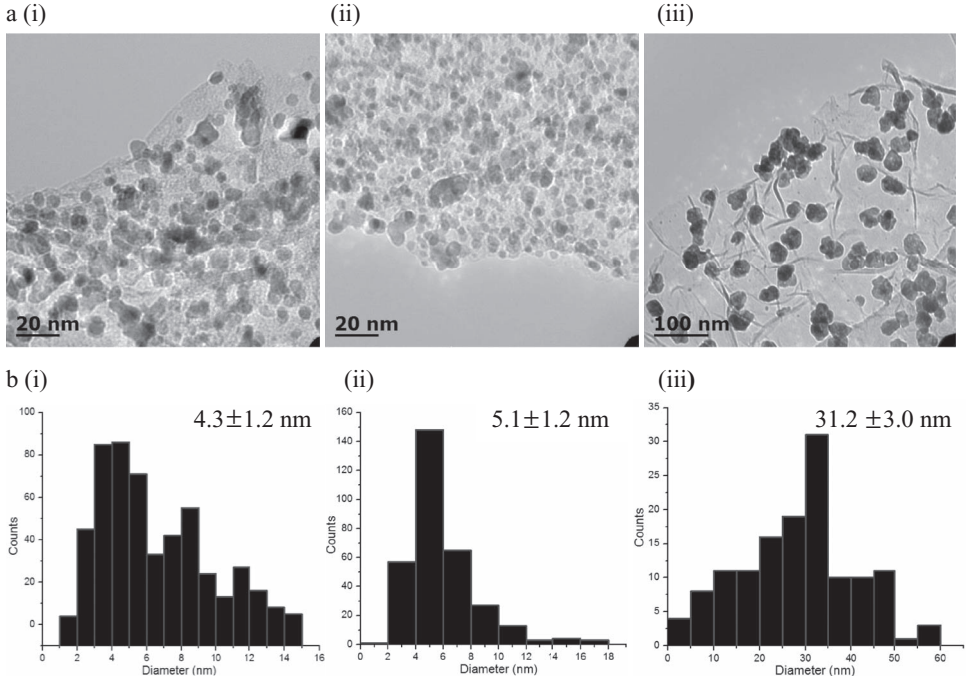

Figure 5. a) TEM micrographs and b) particle size distribution of 30 wt% Pd/3D-GNS synthesized by SARM with () EtOH, (ii)) IPA or (iii) MeOH as a solvent/reducing agent.

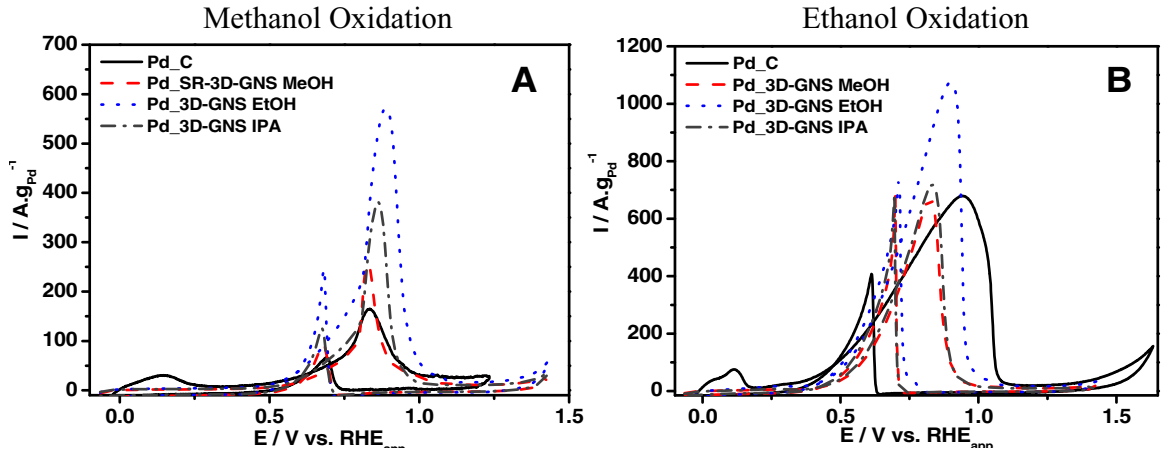

Figure 6. Cyclic voltammograms of 30 wt% Pd-based catalysts: Pd/XC72R (-), Pd/3D-GNS-MeOH (- - -), Pd/3D-GNS-EtOH (· · ·) and Pd/3D-GNS-IPA (- · -) in 1 M MeOH (A) or 1 M EtOH (B) - containing electrolyte. Conditions: catalyst loading – 200 μg cm^{-2}, electrolyte: 1 M KOH, ω = 1600 RPM, v = 20 mV s^{-1}.

In order to investigate the effect of the 3D-GNS support morphology on the materials catalytic activity, we compared it with 2D-GNS that was deposited with 30 wt% Pd using SARM-EtOH fabrication process. As it can be seen from Figure 7, the Pd/2D-GNS catalyst featured a significantly lower peak current density of around 500 A g_{Pd}^{-1} when compared to Pd-3D-GNS EtOH for ethanol oxidation. This demonstrates that for the same Pd loading of 30 wt%, the defective and porous 3D structure of the modified graphene sheets potentially affects the Pd particles distribution, their size and shape. This phenomenon is under further studies in our laboratory.

Catalytic durability and stability of the Pd/3D-GNS for ethanol oxidation reaction was investigated by constant potential tests in 1M KOH+1M C_2H_5OH solution. Similar test was repeated for Pd/2D-GNS for comparison. It can be seen from Figure 8, that both catalysts show a monotonously decaying current density over time, with an initial drop at the stage of 0–200 s. However, the rate of decay slowly starts stabilizing after that stage, where the rate of decay for Pd/3D-GNS was lower than Pd/2D-GNS. Moreover, the current density of Pd/3D-GNS keeps highest in the whole stage compared to Pd/2D-GNS, indicating a higher catalytic stability.

We have investigated the catalytic behavior of materials synthesized from a 1:1 mixture of alcohol: water, by volume. Detailed studies on the influences of the alcohol to water ratios and their effects on the particle sizes and shapes are ongoing, and will be the subject of forthcoming publications.

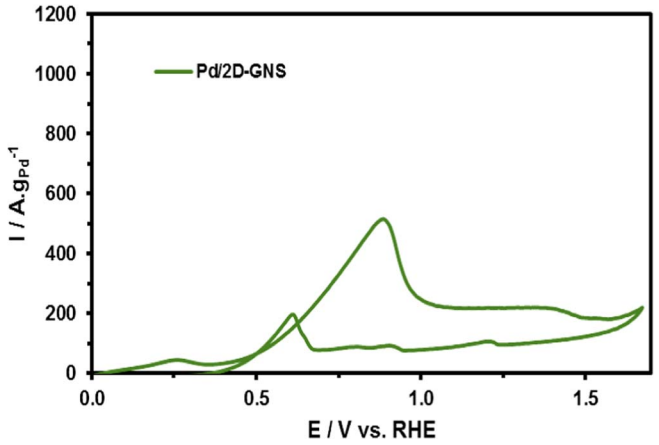

Figure 7. Cyclic voltammograms of 30 wt% Pd supported on 2D-Graphene catalyst for Ethanol oxidation. Conditions: catalyst loading – 200 μg cm^{-2}, electrolyte: 1 M KOH, ω = 1600 RPM, v = 20 mV s^{-1}.

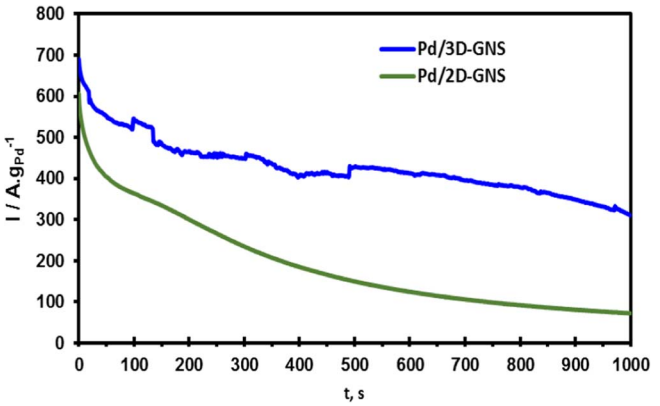

Figure 8. Current–time curves of Pd/3D-GNS and Pd/2D-GNS in the 1M KOH + 1M C_2H_5OH solution.

Conclusions

The Sacrificial Support Method was successfully adopted for the synthesis of highly defective 3-dimensional graphene nano-sheets. This method avoids an excessive washing step in the GO synthesis, which results in batch size increased up to 20 g.

The Soft Alcohol Reduction Method was developed for the deposition of Pd nanoparticles on the surface of 3D-GNS. It was found that the usage of conventional reduction agents such as N_2H_4 or sodium borohydride can be avoided. SARM allows for the synthesis of nanoparticles at room temperature, giving substantial advantages to high-temperature thermal reduction or polyol methods.

The combination of SSM and SARM fabrication processes allowed to rationally synthesize thermally reduced 3D-Graphene nanosheets supports with desirable properties for the development of highly active Pd based electrocatalysts for alcohols electrooxidation.

Acknowledgments

This work was supported by US DOD, ARO-Multi-University Research Initiative grant W911NF-14-1-0263 to University of Utah.

References

1. S. Wasmusa and A. Küver, *J. Electroanal. Chem.*, **461**, 14 (1999).
2. S. Song and P. Tsiakaras, *A. Catal. B.*, **63**, 187 (2006).
3. A. Serov and C. Kwak, *Appl. Catal. B.*, **97**, 1 (2010).
4. X. Yu and P. G. Pickup, *J. Power Sources*, **182**, 124 (2008).
5. A. Serov and C. Kwak, *Appl. Catal. B.*, **98**, 1 (2010).

6. A. Serov and C. Kwak, *Appl. Catal. B.*, **91**, 1 (2009).
7. U. B. Demirci and P. Miele, *Energy Environ. Sci.*, **2**, 627 (2009).
8. E. Antolini and E. R. Gonzalez, *J. Power Sources*, **195**(11), 3431 (2010).
9. S. Spendelow and A. Wieckowski, *Phys. Chem. Chem. Phys.*, **9**(**21**), 2654 (2007).
10. E. Antolini, *Energy Environ. Sci.*, **2**, 915 (2009).
11. R. M. Modibedi, T. Masombuka, and M. K. Mathe, *Int. J. Hydrogen Energy*, **36**, 4664 (2011).
12. W. Du, K. E. Mackenzie, D. F. Milano, N. A. Deskins, D. Su, and X. Teng, *ACS Catalysis*, **2**, 287 (2012).
13. E. E. Switzer, T. S. Olson, A. K. Datye, P. Atanassov, M. R. Hibbs, and C. J. Cornelius, *Electrochim. Acta*, **54**, 989 (2009).
14. Z. Zhang, L. Xin, K. Sun, and W. Li, *Int. J. Hydrogen Energy*, **36**, 12686 (2011).
15. T. Maiyalagan and K. Scott, *J. Power Sources*, **195**, 5246 (2010).
16. U. Martinez, A. Serov, M. Padilla, and P. Atanassov, *ChemSusChem*, **7**(8), 2351 (2014).
17. A. Zalineeva, A. Serov, M. Padilla, U. Martinez, K. Artyushkova, S. Baranton, C. Coutanceau, and P. Atanassov, *J. Am. Chem. Soc.*, **136**, 3937 (2014).
18. A. Serov, U. Martinez, and P. Atanassov, *Electrochem. Comm.*, **34**, 185 (2013).
19. C. Bianchini and P. K. Shen, *Chem. Rev*, **109**, 4183 (2009).
20. N. Mackiewicz, G. Surendran, H. Remita, B. Keita, G. Zhang, L. Nadjo, A. Hagège, E. Doris, and C. Mioskowski, *J. Am. Chem. Soc.*, **130**, 8110 (2008).
21. Z. Wena, S. Yangb, Y. Liang, W. He, H. Tong, L. Hao, X. Zhang, and Qijun Song, *Electrochimica Acta*, **56**, 139 (2010).
22. M. Zhang, J Xie, Q Sun, Z. Yan, M. Chen, J. Jing, and A. M. Hossain, *Electrochimica Acta*, **111**, 855 (2013).
23. W. Liu, A. Herrmann, D. Geiger, L. Borchardt, F. Simon, S. Kaskel, N. Gaponik, and A. Eychmüller, *Angew. Chem. Int. Ed.*, **51**, 5743 (2012).
24. L. Castanheira, L. Dubau, M. Mermoux, G. Berthomé, N. Caqué, E. Rossinot, M. Chatenet, and F. Maillard, *ACS Catal.*, **4**, 2258 (2014).
25. E. Guilminot, A. Corcella, F. Charlot, F. Maillard, and M. Chatenet, *J. Electrochem. Soc.*, **154**, B96 (2007).
26. L. Dubau, F. Maillard, M. Chatenet, L. Guetaz, J. Andre, and E. Rossinot, *J. Electrochem. Soc.*, **157**, B1887 (2010).
27. Z. Zhao, L. Dubau, and F. Maillard, *J. Power Sources*, **217**, 449 (2012).
28. P. J. Ferreira, G. J. la O', Y. Shao-Horn, D. Morgan, R. Makharia, S. Kocha, and H. A. Gasteiger, *J. Electrochem. Soc.*, **152**, A2256 (2005).
29. W. S. Hummers and R. E. Offeman, *J. Am. Chem. Soc.*, **80**(6), 1339 (1958).